Research Article | Vol. 29, No. 16 / 2 August 2021 / Optics Express 24592
Optics EXPRESS

SI-traceable frequency dissemination at 1572.06 nm in a stabilized fiber network with ring topology

Dominik Husmann,[1,*] Laurent-Guy Bernier,[1] Mathieu Bertrand,[2] Davide Calonico,[3] Konstantinos Chaloulos,[4] Gloria Clausen,[5] Cecilia Clivati,[3] Jérôme Faist,[2] Ernst Heiri,[4] Urs Hollenstein,[5] Anatoly Johnson,[6] Fabian Mauchle,[4] Ziv Meir,[6] Frédéric Merkt,[5] Alberto Mura,[3] Giacomo Scalari,[2] Simon Scheidegger,[5] Hansjürg Schmutz,[5] Mudit Sinhal,[6] Stefan Willitsch,[6] and Jacques Morel[1]

[1]*Federal Institute of Metrology METAS, Lindenweg 50, 3003 Bern-Wabern, Switzerland*
[2]*ETH Zurich, Institute for Quantum Electronics, Auguste-Piccard-Hof 1, CH- 8093 Zurich, Switzerland*
[3]*INRIM Istituto Nazionale di Ricerca Metrologica, I- 10135 Torino, Italy*
[4]*SWITCH, Werdstrasse 2, 8021 Zurich, Switzerland*
[5]*ETH Zurich, Laboratory of Physical Chemistry, CH- 8093 Zurich, Switzerland*
[6]*Department of Chemistry, University of Basel, Klingelbergstrasse 80, 4056 Basel, Switzerland*
[*]*dominik.husmann@metas.ch*

Abstract: Frequency dissemination in phase-stabilized optical fiber networks for metrological frequency comparisons and precision measurements are promising candidates to overcome the limitations imposed by satellite techniques. However, in an architecture shared with telecommunication data traffic, network constraints restrict the availability of dedicated channels in the commonly-used *C-band*. Here, we demonstrate the dissemination of an SI-traceable ultrastable optical frequency in the *L-band* over a 456 km fiber network with ring topology, in which data traffic occupies the full *C-band*. We characterize the optical phase noise and evaluate a link instability of 4.7×10^{-16} at 1 s and 3.8×10^{-19} at 2000 s integration time, and a link accuracy of 2×10^{-18}. We demonstrate the application of the disseminated frequency by establishing the SI-traceability of a laser in a remote laboratory. Finally, we show that our metrological frequency does not interfere with data traffic in the telecommunication channels. Our approach combines an unconventional spectral choice in the telecommunication *L-band* with established frequency-stabilization techniques, providing a novel, cost-effective solution for ultrastable frequency-comparison and dissemination, and may contribute to a foundation of a world-wide metrological network.

© 2021 Optical Society of America under the terms of the OSA Open Access Publishing Agreement

1. Introduction

Precise dissemination of accurate frequency signals traceable to the SI definition of the second is essential in many scientific fields, such as precision spectroscopy [1–4], remote clock comparisons in fundamental metrology [5–8], relativistic geodesy [9,10], or synchronization in large-scale facilities [11–13]. In particular, a redefinition of the SI second, as is currently under evaluation, necessitates the comparison of state-of-the-art optical clocks with 10^{-18} relative frequency uncertainty [14]. Most of these applications require higher resolution than allowed by established satellite techniques based on two-way time and frequency transfer (TWTFT) or global navigation satellite systems (GNSS), which achieve fractional frequency stabilities at the 10^{-16} level with measurement times of a few days [15].

#427921 https://doi.org/10.1364/OE.427921
Journal © 2021 Received 19 Apr 2021; revised 1 Jul 2021; accepted 3 Jul 2021; published 19 Jul 2021

Optics EXPRESS

To overcome the limitations of satellite-based frequency comparison techniques, several phase-stabilized optical fiber networks for the dissemination of ultra-stable and accurate optical frequencies have been implemented recently [1,3–8,10–13,16–21], spanning thousands of kilometers and providing transfer stabilities of few 10^{-15} at 1 s with ultimate accuracies beyond 10^{-19} [22,23]. The majority of these networks operate in dedicated fibers (*dark fibers*) and are spectrally situated in the International Telecommunication Union Channel 44 (ITU-T CH44, wavelength λ = 1542.14 nm) in the *C-band* (1530 nm to 1565 nm), where the optical loss is minimal and off-the-shelf telecommunication components are available [24]. However, the high recurring costs for dark-fiber lease have hindered a wider development of such networks. Sharing the available spectrum of the fiber with other network users by exploiting the dense wavelength division multiplexing (DWDM) architecture can significantly reduce costs. A fixed 100 GHz dark channel in the *C-band* has been implemented in France [23] to integrate the ultra-stable frequency signal within the telecommunications data network. However, network operators may have concerns placing such a fixed alien channel inside the *C-band*, where most advanced network architectures use coherent transceivers with flexible spectrum allocation for the various signals based on re-configurable add-drop multiplexers (ROADM). With increasing bandwidth demands of 100 GHz per channel and beyond, transceivers require availability of large blocks of continuous spectrum, which may conflict with the presence of the unmovable alien channel potentially blocking future upgrades. Furthermore, optical networks often incorporate highly integrated amplification structures, which do not a priori account for accommodation of alien signals in the *C-band*. The growing network occupancy of the *C-band* and the restrictions imposed by modern optical fiber network infrastructure thus limit the availability of dedicated metrology channels and leading to higher rental costs. Hence, alternatives in less densely occupied spectral bands need to be explored and validated.

Here, we report the realization of a stabilized frequency-metrology network in Switzerland (see Fig. 1(a) and (b)), spanning over 456 km of optical fibers, and operating in the *L-band* (1565 nm to 1625 nm, see Fig. 1(c)) in ITU-T CH07 (1572.06 nm). The metrological frequency channel allows the dissemination of an ultrastable SI-traceable frequency between dedicated research institutes. The metrological signal is hosted in the same fiber as the data traffic of the Swiss National Research and Education Network (NREN) operated by SWITCH, which lies entirely in the *C-band*. The choice of ITU-T CH07 considers both the advantage provided by a channel outside the *C-band* as discussed above, and the availability and performance of optical components such as narrow-linewidth diode lasers, erbium-doped fiber amplifiers (EDFAs) and optical add-drop multiplexers (OADM). Moreover, the spectral separation minimizes the risk of interference to and from the densely used data-traffic channels, which are separated by spectral guard bands of several nanometers. As the optical components were by default not commercially available in the *L-band* at the start of this project, the components used here were specifically tailored to our wavelength by the manufacturers. The growing need for *L-band* components, however, has in the meantime led to an increase in their commercial availability.

The metrology network connects the Swiss Federal Institute of Metrology, METAS, where an SI-traceable optical frequency is generated, with the University of Basel and ETH Zurich, where the disseminated frequency provides a new improved reference for precision spectroscopy laboratories [25–28]. The network consists of three individually phase-stabilized fiber legs laid out in a ring topology (see Fig. 1(a)), which allows for a genuine end-to-end evaluation of the stability and accuracy of the disseminated frequency. We validate this approach by demonstrating an end-to-end instability of 4.7×10^{-16} at 1 s and 3.8×10^{-19} at 2000 s, and a link accuracy of 2×10^{-18} in the disseminated optical frequency over 456 km. As a first application, we show an improvement in the stability of an SI-traceable frequency measurement of a 729 nm laser used in precision spectroscopy in one of the remote stations. The level of improvement renders novel regimes of precision measurements in atomic and molecular physics accessible, facilitating

Optics EXPRESS

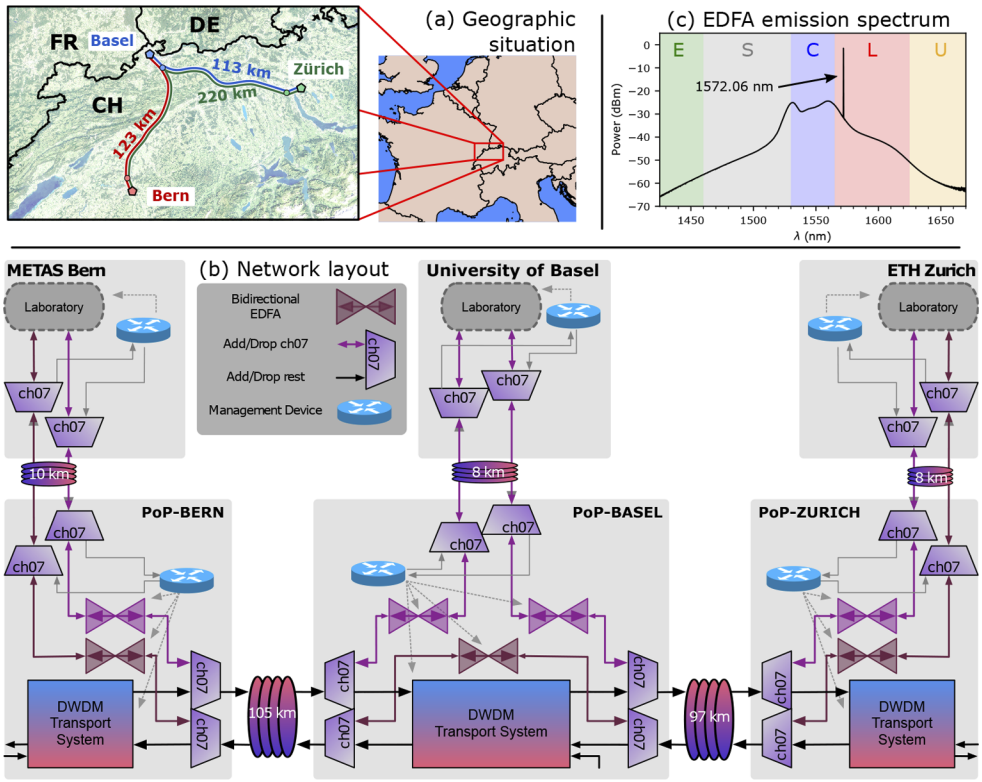

Fig. 1. (a) Geographical situation of the Swiss metrology network connecting institutes in Bern, Basel and Zurich. Each network leg (red, blue and green lines) connects two institutes (big pentagons), and passes through 2-3 network points of presence (PoPs, small circles), where the signal is amplified. (b) Integration of the metrological channel, CH07, into the data network. Purple and brown arrows indicate the bidirectional metrological signal, black arrows indicate the unidirectional data traffic. Bidirectional EDFAs are used to amplify the metrological signal, and 100 GHz wide OADM (ports Add/Drop CH07, Add/Drop rest) filters allow inserting and ejecting the CH07 signal from the SWITCH backbone in the PoPs. Management devices (routers and switches) enable remote control over network and laboratory components (gray arrows). (c) Emission spectrum of the bidirectional erbium-doped fiber amplifier, when injecting a laser at 1572 nm with a power of around −20 dBm, measured with a resolution bandwidth of 0.2 nm. The letters indicate the spectral bands according to ITU-T recommendation.

ways to address fundamental physics questions such as those related to the proton-radius puzzle, a possible variation in time of fundamental constants, and possible extensions of the standard model of particle physics [1,2].

2. Experimental aspects

2.1. Network layout

The three optical fiber legs forming the network (see Tab. 1 and Fig. 1(a)) connect METAS in Bern (BE) to the University of Basel (BS), the University of Basel to ETH Zurich (ZH) and ETH Zurich back to METAS, where the last fiber leg geographically follows the first two fiber segments. The advantage of such a ring network topology lies in the capability for the direct evaluation of the end-to-end optical frequency dissemination uncertainty. Each leg is individually

Optics EXPRESS

stabilized with the well established phase-noise cancellation (PNC) scheme [29–31]. In the master station at METAS, the metrological optical frequency of 190.7 THz (wavelength 1572.06 nm) is prepared and referenced to Coordinated Universal Time (UTC). In the laboratories in Basel and Zurich, the frequency signal is regenerated and sent downstream while part of it is coupled out for local use. The fibers are part of the Swiss NREN (SWITCH). The network implementation is shown in detail in Fig. 1(b). We use DWDM with 100 GHz OADMs to insert and extract the metrological signal with frequency in ITU-T CH07 into the network. The OADMs have typical insertion losses of 0.3 dB to 0.8 dB and provide an isolation of 34 dB to 38 dB. Each leg consists of a long-haul intercity segment, and two shorter urban segments connecting the institutes to point-of-presence (PoP) backbone nodes of the SWITCH network. The transmission losses in the fiber segments between the PoPs, measured for the *C-band* and the *L-band*, are presented in Tab. 1. We attribute the small difference on the order of 2 dB to different measurement methods used for the *C-band* and *L-band*. Power losses in the fibers and in optical add-drop multiplexer modules are compensated using bidirectional EDFAs (*Czech Optical Solutions, CLA BiDi*), which are specifically tailored to 1572 nm (see Fig. 1(c)) by including stronger-erbium-doping fibers to compensate for the reduced gain in the *L-band*. The amplifiers are sandwiched between two OADM filters to suppress amplified spontaneous emission (ASE) outside our 100 GHz channel and to limit self-lasing from amplified reflections [32]. The level of amplification was set for each EDFA individually, with typical values of around 15 dB to 23 dB. Optimally, the input power and amplification for the two directions of a bidirectional EDFAs should be kept symmetric. In our network, the placement of the EDFAs was restricted to the PoPs shown in Fig. 1(a), which did not always allow to satisfy this condition. However we did not encounter any problems arising from this asymmetry. Ultimately, we chose the amplification setting in a way that the optical power in the fiber never exceeded ≈6 dBm in order to reduce detrimental effects from Brillouin and Rayleigh scattering.

Table 1. Overview of the three legs of the stabilized frequency-dissemination network. For each leg, listed are the length, delay limit, number of bidirectional EDFAs, attenuation between the PoPs in the *C-band* and *L-band* (both including the OADM losses), and the net attenuation between the laboratories (including losses from the fibers, connectors, OADMs and gains from the EDFAs, and excluding losses from the PNC part).

	BE - BS	BS - ZH	ZH - BE
Length (km)	123	113	220
delay limit (Hz)	406	442	227
# EDFAs	2	2	3
C-band att. PoP (dB)	25.5	23.6	50.0
L-band att. PoP (dB)	27.2	25.0	52.6
L-band net att. Lab (dB)	0.2	3.1	1.6

2.2. Master and regeneration lasers

The main components of the stabilized laser, the PNC systems, and the regeneration stations at the three laboratories are depicted in Fig. 2. The regeneration stations and PNC systems presented here were designed and built by Istituto Nazionale di Ricerca Metrologica (INRIM). The stable frequency at METAS is generated by locking an external-cavity diode laser (*RIO Planex*) at a wavelength of 1572.06 nm to an ultra-low expansion (ULE) cavity of finesse 13'000 using a Pound-Drever-Hall locking scheme. This laser acts as the master and its frequency is

Optics EXPRESS

continuously measured against an SI-referenced frequency comb (*FC1500-250-ULN, Menlo Systems*). Slow drifts in the laser frequency due to residual thermal relaxation of the cavity are compensated using a digital feedback loop acting on an acousto-optic modulator (AOM). The optical frequency comb is referenced by an active maser, which contributes to the realization of the Swiss timescale UTC(CH) and provides a short-term instability of 1.7×10^{-13} at 1 s. The phase of the maser is regularly compared to the International Atomic Time (TAI) via UTC(CH). This comparison allows us to determine the drift of the maser and thus to estimate its absolute frequency traceable to the SI definition of the second at all times. The stable and traceable optical frequency is then fed into a phase-stabilized link to the next terminal in Basel. The offset-locked regeneration lasers at the University of Basel and ETH Zurich are identical: a local external cavity diode laser (*RIO Planex*) with a free-running specified Lorentzian linewidth of around 2 kHz is phase locked to the incoming optical signal with an offset frequency of −60 MHz, given by the beat signal detected on photodiodes $\mathrm{PD}_{\mathrm{L}}^{\mathrm{BS}}$ and $\mathrm{PD}_{\mathrm{L}}^{\mathrm{ZH}}$. The signal-to-noise ratio (SNR) of this signal is typically 50 dB at a resolution bandwidth of 100 kHz. The bandwidth of the offset lock is set to few tens of kilohertz, which ensures an efficient suppression of the local diode laser noise while preventing spurious noise contributions caused by detection noise, servo bump of the cavity-stabilized laser at around 100 kHz and general broadband electronic noise to enter the loop. A part of the signal from the regeneration laser is split out for local use (e.g. locking an optical frequency comb, see Sec. 3.3 below), while the remainder is injected into the subsequent PNC system and sent further downstream. In both regeneration stations, a Global Positioning System disciplined (GPSD) Rb clock (*SRS FS725 Rb standard* disciplined to *Symmetricom GPS-500* (Basel) or *Spectrum Instruments TM-4* (Zurich)) is used as a local oscillator.

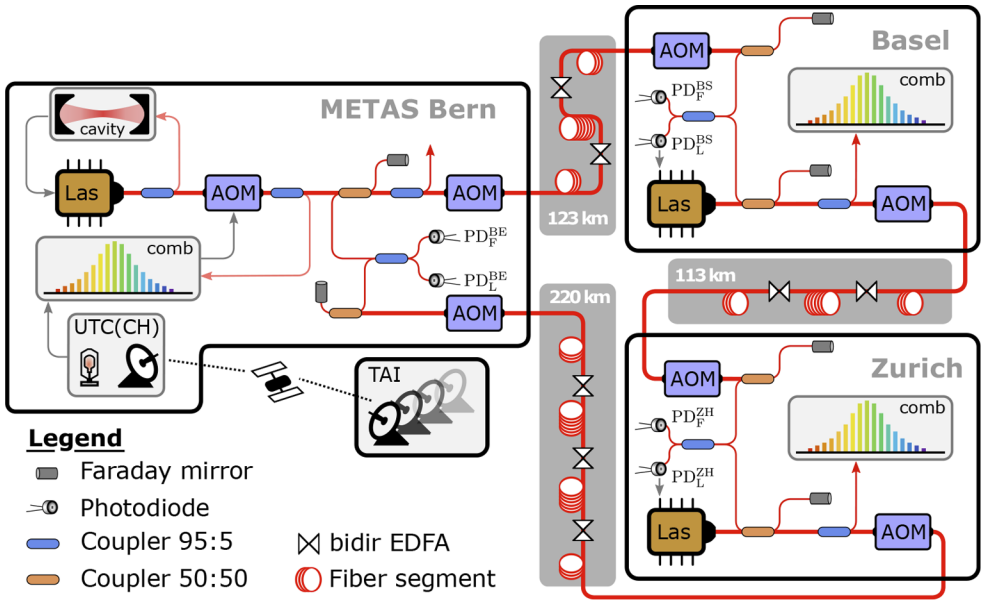

Fig. 2. Detailed schematic of the optical layout: Master station METAS Bern (BE) with traceability to TAI via UTC(CH), regeneration stations at University Basel (BS) and ETH Zurich (ZH), and phase-noise cancellation (PNC) systems with corresponding acousto-optic modulators (AOMs). Optical attenuation in the three fiber legs (gray areas) is compensated using bidirectional EDFAs. Two photodiodes per station detect the fiber PNC beat (F) and laser beat (L) signals. Each station hosts a laser (Las) at 1572.06 nm and an optical frequency comb (comb). Electronic components for signal processing are omitted in the figure for clarity.

Optics EXPRESS

2.3. Phase-noise cancellation

Each of the three stations hosts a PNC system that stabilizes the subsequent fiber leg between the local and a remote station. The PNC system consists of a first AOM (35 MHz) at the local end that applies a frequency correction to the outgoing signal. At the remote end, a second AOM shifts the incoming signal by a fixed frequency of 45 MHz. A coupler with a Faraday mirror reflects part of the signal back to the local end (see Fig. 2). The second AOM allows one to distinguish the full two-way round-trip signal from detrimental reflections. The AOM frequencies are chosen to be incommensurate with the PNC full-round-trip beat note at $2\times(35\ \text{MHz}+45\ \text{MHz}) = 160$ MHz in order to prevent amplitude modulation from spurious reflections in the fiber link. Note that the net frequency shift between two consecutive stations in the network, given by the AOM frequencies and the offset lock frequency, is $35\ \text{MHz}+45\ \text{MHz}-60\ \text{MHz} = 20$ MHz, and the frequency shift of the signal that travels around the full loop is $3\times(35\ \text{MHz}+45\ \text{MHz})-2\times60\ \text{MHz} = 120$ MHz.

The round-trip signal of each of the PNC arms is overlapped with a local copy of the original signal in an all-fiber Michelson-type interferometer, and the beat signal is detected with the photodiodes $\text{PD}_\text{F}^\text{BE}$, $\text{PD}_\text{F}^\text{BS}$ and $\text{PD}_\text{F}^\text{ZH}$, with typical SNR of the beat note of 35 dB at a resolution bandwidth of 100 kHz. Two tracking voltage-controlled oscillators (VCO) at each station are locked to this beat signal by phase-locked loops (PLL) allowing noise rejection outside the locking bandwidth and thus cleaning of the signal. The phase of the primary VCO is continuously compared to an RF reference (GPSD Rb clock) to extract the fiber phase noise. A proportional-integral (PI) feedback circuit applies a proper frequency correction to the optical signal via the local AOM that stabilizes its frequency against the detected perturbations. The PI parameters are matched to the fiber length by ensuring the 0 dB gain to be at a frequency below the delay limit (see Sec. 3.1). The second auxiliary VCO has a slightly different locking bandwidth and is used as a redundant counter that enables to spot cycle slips (CS) [17] in the PNC.

3. Results and discussion

3.1. Phase-noise measurement

We characterized the phase-noise cancellation on the three individual fiber legs by measuring the in-loop phase-noise power spectral density (PSD) of their respective 160 MHz beat signals detected on $\text{PD}_\text{F}^\text{BE}$, $\text{PD}_\text{F}^\text{BS}$ and $\text{PD}_\text{F}^\text{ZH}$. The results are presented in Fig. 3(a). We see qualitative congruence between the three fiber legs. In absence of PNC, the noise spectrum is dominated by white frequency noise. We observe an increased noise around 10 Hz, similar to what was observed in other long-haul fiber links [17,33] where it had been attributed to frequencies originating from buildings and infrastructure. The PNC efficiently suppresses noise at frequencies below the delay limit of $1/(4t_\text{d})$ [18] where t_d is the one-way delay time of the signal passing through the fiber. In the case of our network, this delay limit amounts to 406 Hz, 442 Hz and 227 Hz for the three network legs (see Tab. 1). The feedback loop gain for each fiber segment was chosen as a trade-off between an efficient low-frequency noise suppression and increased noise peaks around the delay-limited servo bandwidth.

Though the in-loop phase-noise measurement gives an indication of the overall fiber noise and the spectral response of the PNC, it carries insufficient information about the actual phase noise on the receiver end. In order to perform an end-to-end comparison of the frequency stability, we exploited the ring topology of our network and measured the phase noise of the return signal with respect to the original signal in Bern by detecting their beat on $\text{PD}_\text{L}^\text{BE}$. The resulting phase noise PSD of this 120 MHz beat signal is shown in Fig. 3(b). Analogous to the results in Fig. 3(a), noise is efficiently rejected for frequencies below around 100 Hz, which is slightly below the delay limit of the longest leg (ZH-BE). In spectral regions dominated by white frequency noise, this leads to a flat curve limited by delay-unsuppressed residual phase noise. We compare this to

Optics EXPRESS

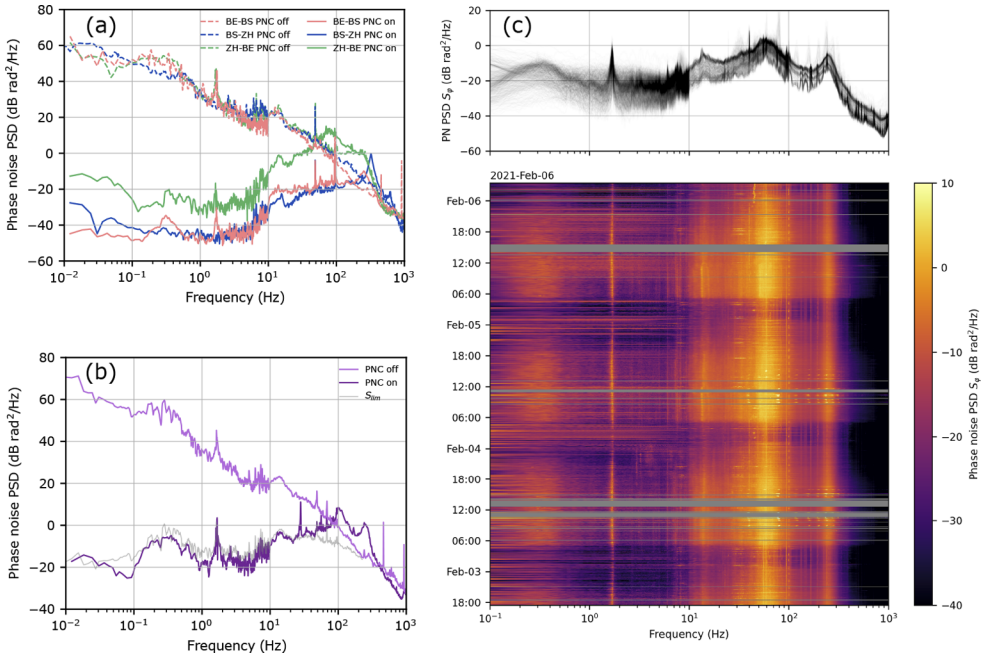

Fig. 3. (a) Phase noise PSD of the 160 MHz round-trip PNC beat note of the three fiber segments BE-BS (red), BS-ZH (blue) and ZH-BE (green), with PNC on (solid lines) and off (dashed lines). (b) Phase noise PSD of the 120 MHz end-to-end beat note between the local laser at METAS and the return signal from Zurich, with PNC off (light magenta) and on (dark magenta). Gray curve: theoretical limit imposed by delay-unsuppressed noise of the longest fiber leg ZH-BE. (c) Same signal as in (b) in stabilized condition, measured over several days in February 2021 in intervals of around 6 min. The upper panel shows all measurements superimposed onto each other. The lower panel shows a 2D view of the same data, with the y-axis representing time. Day-night cycles are distinctly visible as alternating high- and low-noise periods. Traces with excessive CS leading to high phase noise at low frequencies are omitted from the upper panel and masked in gray in the lower panel.

the theoretical limit of ideal noise rejection $S_{\mathrm{lim}}(f)$ [18] (gray curve in Fig. 3(b)) for the longest fiber segment of 220 km, under the assumption that noise is uncorrelated with position. The theoretical limit matches the measurement for frequencies below the servo bump, confirming that the noise suppression works at its optimum. We consider the phase noise in Fig. 3(b) to be an upper bound for the phase noise of individual segments.

The fibers used in this project are typically installed close to main traffic routes, and are thus expected to be subjected to temporal fluctuations in environmental anthropogenic noise. We analyzed this by measuring the phase noise of the end-to-end beat over several days, in intervals of roughly 6 min. The results are presented in Fig. 3(c) and show distinct day-night oscillations: At around 5 am, there is a sharp increase in phase noise extending over the full spectrum. In the late afternoon we observe a gradual decrease in phase noise, leading to a minimum during the night. We attribute this evolution to environmental noise given by human activity and transport-system behavior reflecting typical work-day schedules. The distinct peak in phase noise at 1.7 Hz originates from a fiber segment between Bern and Basel (see also Fig. 3(a)). While its origin is not known, we consider resonances of particular infrastructures such as bridges or rotating fans in power plants located in the vicinity of the fiber as possible sources.

Optics EXPRESS

3.2. Long-term stability of the link

We analyzed the long-term stability of the fiber link by monitoring the full-loop end-to-end beat frequency on PD_L^{BE} using a dead-time free counter (*K+K FXE80*) [34]. In a first set of experiments, we measured for around 700 s with a sampling rate of 1 kHz. In a second set of measurements, we monitored the beat frequency over several hours, during which we selected the internal $\Lambda-$ averaging mode of the frequency counter to reduce the sampling rate from 1 kHz to 1 Hz and to reduce the equivalent measurement bandwidth. For comparison, we repeated this measurement for the unstabilized link. The results are presented in Fig. 4(a), and show a link instability of 4.7×10^{-16} at 1 s measurement time. The overlapping Allan deviation (ADEV) of the stabilized link shows a $1/\tau$ dependence for a CS-free data segment, which is a typical behavior for fiber links affected by phase noise in the acoustic range [17,30,35], and reaches a noise floor of 3.8×10^{-19} at 2000 s. Owing to a different transfer function, the modified Allan deviation (MDEV) is predicted to exhibit a stronger $1/\tau^2$-dependence in presence of noise processes like blue phase noise, spurs, and bumps [17,35], which are processes we also observe for our

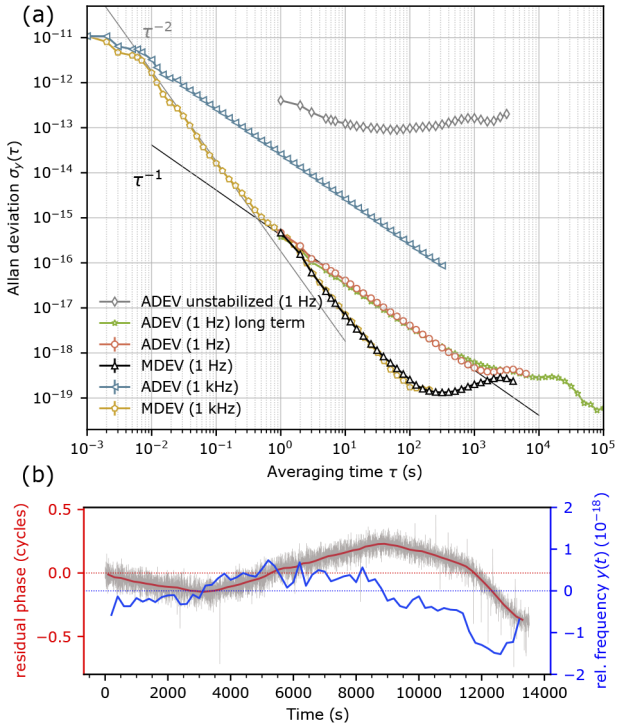

Fig. 4. (a) Allan deviation of the end-to-end beat frequency of the stabilized link. Red: ADEV with 1 Hz sampling in $\Lambda-$ type averaging mode. Black: MDEV of the same data in red. Blue: ADEV with 1 kHz sampling. Yellow: MDEV with 1 kHz sampling of the same data in blue. Gray: ADEV of the unstabilized link with 1 Hz sampling. The gray straight line is a $1/\tau^2$ fit to a subset of the yellow data points. The black straight line is a $1/\tau$ fit to a subset of the red data points. Green: ADEV with 1 Hz sampling, measured over several days. In contrast to the blue and red data, which are free of CS, here we have suppressed an average of 4.7 CS per hour. (b) Gray: Residual phase evolution, based on the same 1 Hz sampled data set from (a) (red and black symbols). Red: moving average of the gray curve, with averaging window length of 200 s. Blue: derivative of the red curve, corresponding to the deviation of the relative frequency from the nominal frequency. The magnitude of these excursions give an estimate of the frequency uncertainty introduced by the link.

Optics EXPRESS

stabilized link between 5 Hz and 100 Hz (see Fig. 3(b)). This prediction is in agreement with the $1/\tau^2$ we observe for the MDEV in Fig. 4(a), averaging down to the instability floor of 1.3×10^{-19} in 300 s. The MDEVs at 1 kHz and 1 Hz can be concatenated at $\tau = 1$ s, in agreement with the fact that the low-pass filtering of the $\Lambda-$ type averaging of the frequency counter is equivalent to the filtering performed in the calculation of the MDEV [35]. Further we have evaluated the ADEV of a data set measured over several days at 1 Hz sampling. Here we have recorded an average of 4.7 CS per hour. We have suppressed these and the directly adjacent data points in the calculation of the ADEV. Owing to the occurrence of CS, the ADEV here shows flattening at integration times of few hundreds of seconds, roughly corresponding to the CS rate. Further we observe a decrease of the ADEV below 1×10^{-19} for integration times of around 1 day, indicating averaging out of diurnal fluctuations.

The stability analysis does not account for systematic shifts with respect to the nominal frequency, which may occur due to drifts in the uncompensated interferometer arms. To estimate these systematic deviations, we measured the relative frequency deviation from the nominal value for a CS-free segment measured over 13 500 s (see Fig. 4(b)). We attribute these excursions to daily temperature variations in the uncompensated interferometer arms. The typical frequency excursions are of the order of 1×10^{-18}, based on which we determine a conservative limit of the link accuracy to be 2×10^{-18} under the assumption that residual interferometer noise in the individual stations is uncorrelated. For the application of frequency dissemination to remote stations, the current achieved link instability is two orders of magnitude lower than the intrinsic uncertainty of the disseminated frequency, and thus does not represent a limitation. Nevertheless, for further upgrades, the link stability and accuracy could be improved by a refined design of the interferometer, e.g., designing a fully balanced interferometer [23,36].

3.3. SI-referencing a 729 nm spectroscopy laser at a remote station

As a demonstration of the application of the frequency-dissemination network, we establish SI-traceabiltiy of the frequency of a narrow-linewidth near-infrared spectroscopy laser at 729 nm in the remote station at the University of Basel by referencing it to the frequency standard at METAS (see Fig. 5(a) for the locking setup). The short-term linewidth of the 729 nm laser in Basel was stabilized by a lock to a local high-finesse ULE cavity. Without further corrections, the long-term instability was limited by the drifts of the ULE cavity of ~15 mHz/s (light-red trace in Fig. 5(b)). We used the beat signal of the referenced regeneration laser with the local comb at 1572.06 nm to track the slow drifts of the ULE cavity and subsequently compensate for them via a digital feedback loop acting on an AOM in the spectroscopy-laser path to the cavity (see Fig. 5(a)). In this way, we obtained both a narrow short-term linewidth and an improved long-term stability of the laser (Fig. 5(b) red traces) that is traceable to the SI definition of the second as a prerequisite for applications in precision spectroscopy.

To illustrate the improved frequency measurement of the spectroscopy laser, the frequency of the laser was determined by two methods, i.e., first, by referencing its frequency to the local GPSD Rb clock, or second, by referencing it to the frequency disseminated from METAS. In either case, the frequency comb was optically locked to the 729 nm laser. In the first method, the frequency was given by

$$f_{729} = 2f_{\mathrm{CEO}} + n_{729}f_{\mathrm{rep}} + f_{729}^{\mathrm{beat}}. \tag{1}$$

Here, f_{CEO} and f_{rep} are the carrier-envelope-offset frequency (CEO) and the repetition-rate of the frequency comb, respectively, $n_{729} = 1'644'167$ is the index of the frequency-comb tooth used to create a beat with the spectroscopy laser at frequency f_{729}^{beat}. All measured frequencies were referenced to the local GPSD Rb clock. The factor of 2 appears with f_{CEO} because the spectrum of the comb is doubled in order to beat with the 729 nm laser. The limiting factor in this method was the repetition-rate instability as measured by the GPSD Rb clock due to the

Optics EXPRESS

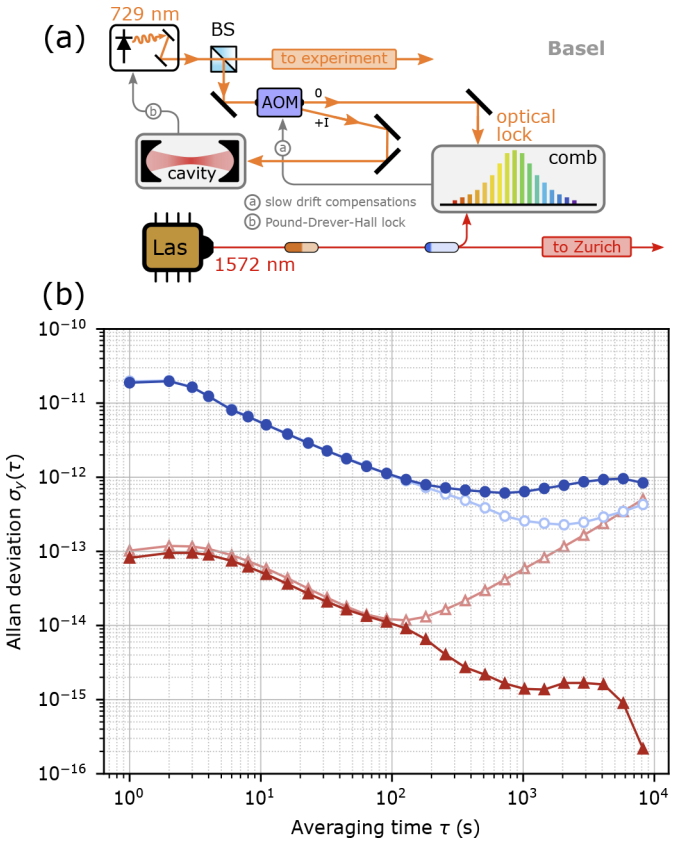

Fig. 5. (a) Compensation setup for improving the long-term stability of a 729 nm spectroscopy laser in the remote station in Basel. (b) Allan deviation of the frequency of a spectroscopy laser (729 nm) in the Basel remote station determined by two methods. For the blue circles, the laser frequency is referenced to a local GPSD Rb standard (Eq. (1)). For the red triangles, the laser frequency is referenced to the METAS standard via the fiber link (Eq. (2)). The light-blue and light-red traces were obtained after the compensation for the slow drifts of the ULE cavity in Basel was turned off. Differences between the light and thick red traces at short times (<100 s) and the light and thick blue traces at long times (>100 s) are due to non-stationary effects, such as changes in the gain of the laser locks (red curves) and drifts of the Rb clock compared to the GPS (blue curves).

large multiplication factor, n_{729}. In the second method, the frequency was given by

$$f_{729} = (2 - x)f_{\mathrm{CEO}} + x(f_{1572} - f_{1572}^{\mathrm{beat}}) + f_{729}^{\mathrm{beat}}. \tag{2}$$

Here, f_{1572} is the frequency of the regeneration laser which was determined by METAS, f_{1572}^{beat} is the beat frequency with the local frequency-comb tooth, $n_{1572} = 762'813$, and $x = n_{729}/n_{1572} \approx 2.16$. With this type of frequency ratio method [37], the local-frequency-comb repetition rate does not appear in the frequency comparison since we make a comparison between two optical frequencies. The limiting factor in this method is the instability of the disseminated frequency manifested in the link beat with the local frequency comb, f_{1572}^{beat}.

In Fig. 5(b), we show plots of the Allan deviation of the 729 nm laser frequency obtained by both methods. In the first method (blue traces), the instability of the Rb clock limits the frequency determination to $\sim 5 \times 10^{-13}$ at 1000 s. The METAS standard delivered via the fiber link, however, provides more than two orders of magnitude reduction of instability of the laser

Optics EXPRESS

over the averaging time analyzed here (thick red trace). Already at an averaging time of 1000 s, the statistical uncertainty of $\sim 1 \times 10^{-15}$ is better than the instability originating from the METAS standard compared to TAI.

The Allan deviation of the link exhibits a plateau up to 5 s integration time. This behavior is attributed to the time constant of the lock of the master laser to the SI-referenced frequency comb at METAS and the instability of the ULE cavity at METAS which has higher drifts and a lower finesse compared to the cavity used in Basel. The small shoulder at 100 s is a reminiscence of the ULE cavity in Basel. The maximum at 3000 s is attributed to the feedback loop of the slow-drift compensation in Basel.

3.4. Bit error rate measurement on the data traffic channels

Multiplexing a new frequency channel into an existing data network requires careful evaluation of potential cross talk with the existing channels. In order to verify that our metrological signal in ITU-T CH07 does not disturb the existing data-communication channels in the *C-band*, we exploited the integrated error detection and correction schemes (forward error correction) of the optical transponder systems in selected data traffic channels of the SWITCH network infrastructure. To this end, we observed the rate of corrected errors per second in the transponders over 2-3 days both in presence and absence of the metrological signal in the network, with the report interval of the transponders set to 15 min. The measurement was performed on 14 different optical channels varying in fiber segments, frequency and data modulation schemes. All channels maintained error-free communication during the measurement times, demonstrating that all detected errors were corrected by the transponders. Time traces of the rate of corrected errors for 6 exemplary channels are shown in Fig. 6. While there are clear day-to-day fluctuations, the data show no significant impact of our 1572 nm signal on the number of corrected errors in the measured data channels for either of the 14 measurements. This observation validates our choice of a metrological *L-band* frequency and confirms that optical dissemination in the *L-band* does not affect telecommunication data transmission in the *C-band*.

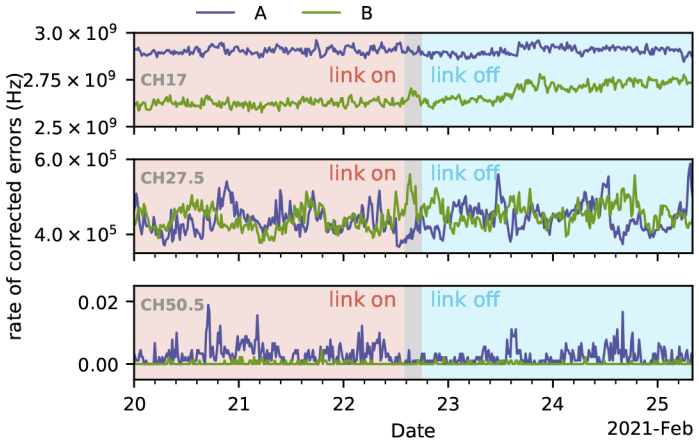

Fig. 6. Rate of corrected errors between two transponders in 3 selected data channels (CH17, CH27.5 and CH50.5) sharing fibers with the metrological signal. Each channel was measured in both directions (lines A and B). In the red (blue) shaded area, the metrological signal was on (off). In the transitions time (gray area), the signal was partially on. The modulation schemes were 200 GBit/s polarization 8 quadrature amplitude modulation (DP-8QAM) for CH17, 100 Gbit/s dual polarization quadrature phase shift keying for CH27.5 and 10 Gbit non-return-to-zero on-off keying for CH50.5.

Optics EXPRESS

4. Conclusion and outlook

The results presented here validate the approach of multiplexing a channel for stabilized metrological-frequency dissemination located in the *L-band* into an existing optical fiber data network. The performance of the network link allows for the dissemination of an SI-traceable frequency without significant degradation in the stability and accuracy. Here we demonstrated the improvement of the frequency reference in a remote laboratory by two orders of magnitude compared to the previously employed GPSD Rb clock standard. As prospective applications of the present frequency-transfer network, we envisage precision spectroscopy of molecular ions [26,38] and of Rydberg atoms and molecules [27,28]. From a metrology viewpoint, the network opens up the potential to compare atomic clocks, such as the Cs primary frequency standard FoCS-2 at METAS [39], to other frequency standards. Furthermore, such a network can be used for frequency comparisons beyond the current instability given by primary frequency standards, such as optical clocks. The frequency-dissemination network presented here offers the advantage of being both cost effective and relatively simple in implementation in an existing fiber network, which is a prerequisite for the development of a world-wide metrological network.

Funding. European Research Council (743121); National Center of Competence in Research Quantum Science and Technology; Schweizerischer Nationalfonds zur Förderung der Wissenschaftlichen Forschung (CRSII5_183579).

Acknowledgments. We thank A. Frank for support with electronics.

Disclosures. The authors declare no conflicts of interest.

Data availability. Data underlying the figures presented in this paper are available in Ref. [40].

References

1. A. Matveev, C. G. Parthey, K. Predehl, J. Alnis, A. Beyer, R. Holzwarth, T. Udem, T. Wilken, N. Kolachevsky, M. Abgrall, D. Rovera, C. Salomon, P. Laurent, G. Grosche, O. Terra, T. Legero, H. Schnatz, S. Weyers, B. Altschul, and T. W. Hänsch, "Precision Measurement of the Hydrogen 1S – 2S Frequency via a 920-km Fiber Link," Phys. Rev. Lett. **110**(23), 230801 (2013).
2. M. S. Safronova, D. Budker, D. DeMille, D. F. Jackson Kimball, A. Derevianko, and C. W. Clark, "Search for new physics with atoms and molecules," Rev. Mod. Phys. **90**(2), 025008 (2018).
3. C. Clivati, G. Cappellini, L. F. Livi, F. Poggiali, M. Siciliani de Cumis, M. Mancini, G. Pagano, M. Frittelli, A. Mura, G. A. Costanzo, F. Levi, D. Calonico, L. Fallani, J. Catani, and M. Inguscio, "Measuring absolute frequencies beyond the GPS limit via long-haul optical frequency dissemination," Opt. Express **24**(11), 11865–11875 (2016).
4. R. Santagata, D. B. A. Tran, B. Argence, O. Lopez, S. K. Tokunaga, F. Wiotte, H. Mouhamad, A. Goncharov, M. Abgrall, Y. Le Coq, H. Alvarez-Martinez, R. Le Targat, W. K. Lee, D. Xu, P.-E. Pottie, B. Darquié, and A. Amy-Klein, "High-precision methanol spectroscopy with a widely tunable SI-traceable frequency-comb-based mid-infrared QCL," Optica **6**(4), 411–423 (2019).
5. C. Lisdat, G. Grosche, N. Quintin, C. Shi, S. M. F. Raupach, C. Grebing, D. Nicolodi, F. Stefani, A. Al-Masoudi, S. Dörscher, S. Häfner, J.-L. Robyr, N. Chiodo, S. Bilicki, E. Bookjans, A. Koczwara, S. Koke, A. Kuhl, F. Wiotte, F. Meynadier, E. Camisard, M. Abgrall, M. Lours, T. Legero, H. Schnatz, U. Sterr, H. Denker, C. Chardonnet, Y. Le Coq, G. Santarelli, A. Amy-Klein, R. Le Targat, J. Lodewyck, O. Lopez, and P.-E. Pottie, "A clock network for geodesy and fundamental science," Nat. Commun. **7**(1), 12443 (2016).
6. P. Delva, J. Lodewyck, S. Bilicki, E. Bookjans, G. Vallet, R. Le Targat, P.-E. Pottie, C. Guerlin, F. Meynadier, C. Le Poncin-Lafitte, O. Lopez, A. Amy-Klein, W.-K. Lee, N. Quintin, C. Lisdat, A. Al-Masoudi, S. Dörscher, C. Grebing, G. Grosche, A. Kuhl, S. Raupach, U. Sterr, I. R. Hill, R. Hobson, W. Bowden, J. Kronjäger, G. Marra, A. Rolland, F. N. Baynes, H. S. Margolis, and P. Gill, "Test of Special Relativity Using a Fiber Network of Optical Clocks," Phys. Rev. Lett. **118**(22), 221102 (2017).
7. F.-L. Hong, M. Musha, M. Takamoto, H. Inaba, S. Yanagimachi, A. Takamizawa, K. Watabe, T. Ikegami, M. Imae, Y. Fujii, M. Amemiya, K. Nakagawa, K. Ueda, and H. Katori, "Measuring the frequency of a Sr optical lattice clock using a 120 km coherent optical transfer," Opt. Lett. **34**(5), 692–694 (2009).
8. Boulder Atomic Clock Optical Network (BACON) Collaboration, K. Beloy, M. I. Bodine, T. Bothwell, S. M. Brewer, S. L. Bromley, J.-S. Chen, J.-D. Deschênes, S. A. Diddams, R. J. Fasano, T. M. Fortier, Y. S. Hassan, D. B. Hume, D. Kedar, C. J. Kennedy, I. Khader, A. Koepke, D. R. Leibrandt, H. Leopardi, A. D. Ludlow, W. F. McGrew, W. R. Milner, N. R. Newbury, D. Nicolodi, E. Oelker, T. E. Parker, J. M. Robinson, S. Romisch, S. A. Schäffer, J. A. Sherman, L. C. Sinclair, L. Sonderhouse, W. C. Swann, J. Yao, J. Ye, and X. Zhang, "Frequency ratio measurements at 18-digit accuracy using an optical clock network," Nature **591**(7851), 564–569 (2021).
9. T. Takano, M. Takamoto, I. Ushijima, N. Ohmae, T. Akatsuka, A. Yamaguchi, Y. Kuroishi, H. Munekane, B. Miyahara, and H. Katori, "Geopotential measurements with synchronously linked optical lattice clocks," Nat. Photonics **10**(10), 662–666 (2016).

Optics EXPRESS

10. J. Grotti, S. Koller, S. Vogt, S. Häfner, U. Sterr, C. Lisdat, H. Denker, C. Voigt, L. Timmen, A. Rolland, F. N. Baynes, H. S. Margolis, M. Zampaolo, P. Thoumany, M. Pizzocaro, B. Rauf, F. Bregolin, A. Tampellini, P. Barbieri, M. Zucco, G. A. Costanzo, C. Clivati, F. Levi, and D. Calonico, "Geodesy and metrology with a transportable optical clock," Nat. Phys. **14**(5), 437–441 (2018).
11. C. Clivati, R. Aiello, G. Bianco, C. Bortolotti, P. De Natale, V. Di Sarno, P. Maddaloni, P. Maddaloni, G. Maccaferri, A. Mura, M. Negusini, F. Levi, F. Perini, R. Ricci, M. Roma, L. S. Amato, M. Siciliani de Cumis, M. Stagni, A. Tuozzi, and D. Calonico, "Common-clock very long baseline interferometry using a coherent optical fiber link," Optica **7**(8), 1031–1037 (2020).
12. Y. He, K. G. H. Baldwin, B. J. Orr, R. B. Warrington, M. J. Wouters, A. N. Luiten, P. Mirtschin, T. Tzioumis, C. Phillips, J. Stevens, B. Lennon, S. Munting, G. Aben, T. Newlands, and T. Rayner, "Long-distance telecom-fiber transfer of a radio-frequency reference for radio astronomy," Optica **5**(2), 138–146 (2018).
13. P. Krehlik, Ł. Buczek, J. Kołodziej, M. Lipiński, Ł. Śliwczyński, J. Nawrocki, P. Nogaś, A. Marecki, E. Pazderski, P. Ablewski, M. Bober, R. Ciuryło, A. Cygan, D. Lisak, P. Masłowski, P. Morzyński, M. Zawada, R. M. Campbell, J. Pieczerak, A. Binczewski, and K. Turza, "Fibre-optic delivery of time and frequency to VLBI station," A&A **603**, A48 (2017).
14. F. Riehle, P. Gill, F. Arias, and L. Robertsson, "The CIPM list of recommended frequency standard values: guidelines and procedures," Metrologia **55**(2), 188–200 (2018).
15. G. Petit, A. Kanj, S. Loyer, J. Delporte, F. Mercier, and F. Perosanz, "1×10⁻16 frequency transfer by GPS PPP with integer ambiguity resolution," Metrologia **52**(2), 301–309 (2015).
16. J. Guéna, S. Weyers, M. Abgrall, C. Grebing, V. Gerginov, P. Rosenbusch, S. Bize, B. Lipphardt, H. Denker, N. Quintin, S. M. F. Raupach, D. Nicolodi, F. Stefani, N. Chiodo, S. Koke, A. Kuhl, F. Wiotte, F. Meynadier, E. Camisard, C. Chardonnet, Y. Le Coq, M. Lours, G. Santarelli, A. Amy-Klein, R. Le Targat, O. Lopez, P. E. Pottie, and G. Grosche, "First international comparison of fountain primary frequency standards via a long distance optical fiber link," Metrologia **54**(3), 348–354 (2017).
17. S. Droste, F. Ozimek, T. Udem, K. Predehl, T. W. Hänsch, H. Schnatz, G. Grosche, and R. Holzwarth, "Optical-Frequency Transfer over a Single-Span 1840 km Fiber Link," Phys. Rev. Lett. **111**(11), 110801 (2013).
18. P. A. Williams, W. C. Swann, and N. R. Newbury, "High-stability transfer of an optical frequency over long fiber-optic links," J. Opt. Soc. Am. B **25**(8), 1284–1293 (2008).
19. O. Lopez, F. Kéfélian, H. Jiang, A. Haboucha, A. Bercy, F. Stefani, B. Chanteau, A. Kanj, D. Rovera, J. Achkar, C. Chardonnet, P.-E. Pottie, A. Amy-Klein, and G. Santarelli, "Frequency and time transfer for metrology and beyond using telecommunication network fibres," C. R. Phys. **16**(5), 531–539 (2015).
20. K. Predehl, G. Grosche, S. M. F. Raupach, S. Droste, O. Terra, J. Alnis, T. Legero, T. W. Hänsch, T. Udem, R. Holzwarth, and H. Schnatz, "A 920-Kilometer Optical Fiber Link for Frequency Metrology at the 19th Decimal Place," Science **336**(6080), 441–444 (2012).
21. M. Fujieda, M. Kumagai, S. Nagano, A. Yamaguchi, H. Hachisu, and T. Ido, "All-optical link for direct comparison of distant optical clocks," Opt. Express **19**(17), 16498–16507 (2011).
22. S. M. F. Raupach, A. Koczwara, and G. Grosche, "Brillouin amplification supports $1 \times 10^{-}20$ uncertainty in optical frequency transfer over 1400 km of underground fiber," Phys. Rev. A **92**(2), 021801 (2015).
23. E. Cantin, M. Tønnes, R. L. Targat, A. Amy-Klein, O. Lopez, and P.-E. Pottie, "An accurate and robust metrological network for coherent optical frequency dissemination," New J. Phys. **23**(5), 053027 (2021).
24. International Telecommunication Union, "Optical Fibres, Cables and Systems," (2009).
25. M. Sinhal, Z. Meir, K. Najafian, G. Hegi, and S. Willitsch, "Quantum-nondemolition state detection and spectroscopy of single trapped molecules," Science **367**(6483), 1213–1218 (2020).
26. M. Germann, X. Tong, and S. Willitsch, "Observation of electric-dipole-forbidden infrared transitions in cold molecular ions," Nat. Phys. **10**(11), 820–824 (2014).
27. M. Beyer, N. Hölsch, J. A. Agner, J. Deiglmayr, H. Schmutz, and F. Merkt, "Metrology of high-n Rydberg states of molecular hydrogen with $\Delta\nu/\nu = 2 \times 10^{-10}$ accuracy," Phys. Rev. A **97**(1), 012501 (2018).
28. M. Peper, F. Helmrich, J. Butscher, J. A. Agner, H. Schmutz, F. Merkt, and J. Deiglmayr, "Precision measurement of the ionization energy and quantum defects of ^{3}9K I," Phys. Rev. A **100**(1), 012501 (2019).
29. L.-S. Ma, P. Jungner, J. Ye, and J. L. Hall, "Delivering the same optical frequency at two places: accurate cancellation of phase noise introduced by an optical fiber or other time-varying path," Opt. Lett. **19**(21), 1777–1779 (1994).
30. N. R. Newbury, P. A. Williams, and W. C. Swann, "Coherent transfer of an optical carrier over 251 km," Opt. Lett. **32**(21), 3056–3058 (2007).
31. G. Grosche, O. Terra, K. Predehl, R. Holzwarth, B. Lipphardt, F. Vogt, U. Sterr, and H. Schnatz, "Optical frequency transfer via 146 km fiber link with 10^{-19} relative accuracy," Opt. Lett. **34**(15), 2270–2272 (2009).
32. J. Vojtech, O. Havlis, S. Bhowmick, M. Slapak, P. Munster, T. Horvath, R. Velc, J. Kundrat, L. Altmannova, R. Vohnout, P. Skoda, and V. Smotlacha, "White Rabbit Single Fibre Bidirectional Transmission of Precise Time Using Unconventional Wavelengths," in *2020 Joint Conference of the IEEE International Frequency Control Symposium and International Symposium on Applications of Ferroelectrics (IFCS-ISAF)*, (2020), pp. 1–4.
33. D. Calonico, E. K. Bertacco, C. E. Calosso, C. Clivati, G. A. Costanzo, M. Frittelli, A. Godone, A. Mura, N. Poli, D. V. Sutyrin, G. Tino, M. E. Zucco, and F. Levi, "High-accuracy coherent optical frequency transfer over a doubled 642-km fiber link," Appl. Phys. B **117**(3), 979–986 (2014).

Optics EXPRESS

34. G. Kramer and W. Klische, "Extra high precision digital phase recorder," in *18th European Frequency and Time Forum (EFTF 2004)*, (2004), pp. 595–602.
35. C. E. Calosso, C. Clivati, and S. Micalizio, "Avoiding Aliasing in Allan Variance: An Application to Fiber Link Data Analysis," IEEE Trans. Ultrason., Ferroelect., Freq. Contr. **63**(4), 646–655 (2016).
36. F. Stefani, O. Lopez, A. Bercy, W.-K. Lee, C. Chardonnet, G. Santarelli, P.-E. Pottie, and A. Amy-Klein, "Tackling the limits of optical fiber links," J. Opt. Soc. Am. B **32**(5), 787–797 (2015).
37. H. Telle, B. Lipphardt, and J. Stenger, "Kerr-lens, mode-locked lasers as transfer oscillators for optical frequency measurements," Appl. Phys. B **74**(1), 1–6 (2002).
38. K. Najafian, Z. Meir, and S. Willitsch, "From megahertz to terahertz qubits encoded in molecular ions: theoretical analysis of dipole-forbidden spectroscopic transitions in N_2^+," Phys. Chem. Chem. Phys. **22**(40), 23083–23098 (2020).
39. A. Jallageas, L. Devenoges, M. Petersen, J. Morel, L. G. Bernier, D. Schenker, P. Thomann, and T. Südmeyer, "First uncertainty evaluation of the FoCS-2 primary frequency standard," Metrologia **55**(3), 366–385 (2018).
40. D. Husmann, L.-G. Bernier, M. Bertrand, D. Calonico, K. Chaloulos, G. Clausen, C. Clivati, J. Faist, E. Heiri, U. Hollenstein, A. Johnson, F. Mauchle, Z. Meir, F. Merkt, A. Mura, G. Scalari, S. Scheidegger, H. Schmutz, M. Sinhal, S. Willitsch, and J. Morel, "Figure data for the manuscript "SI-traceable frequency dissemination at 1572.06 nm in a stabilized fiber network with ring topology," (2021). Zenodo, https://doi.org/10.5281/zenodo.5040076.

131.152.105.95 {ts '2021-12-22 04:21:30'}